IEEE Access
Multidisciplinary ⋮ Rapid Review ⋮ Open Access Journal

Received 29 June 2024, accepted 15 July 2024, date of publication 22 July 2024, date of current version 31 July 2024.

*Digital Object Identifier 10.1109/ACCESS.2024.3431934*

RESEARCH ARTICLE

# Dynamic Performance of a Decoupled Dual Wound Synchronous Generator for Electric Propulsion of Ships

**HAN WANG[1], XIANWU ZENG[1], (Member, IEEE), JOHN FREDERICK EASTHAM[2], BOYUAN YIN[2], AND XIAOZE PEI[2], (Senior Member, IEEE)**

[1]Department of Mechanical Engineering, University of Bath, BA2 7AY Bath, U.K.
[2]Department of Electronic and Electrical Engineering, University of Bath, BA2 7AY Bath, U.K.

Corresponding author: Xiaoze Pei (x.pei@bath.ac.uk)

This work was supported in part by U.K. EPSRC Open Fellowship-Towards Zero Emissions Electric Aircraft through Superconducting DC Distribution Network under Grant EP/W033941/1.

**ABSTRACT** The dual wound generator brings significant advantages to integrated electric propulsion systems in ships, particularly in terms of footprint reduction and space saving. However, prior research on machines using the same pole number for each of the windings has highlighted the challenge of severe magnetic coupling effects between the two outputs when subjected to dynamically changing loads. This reduces the stability of the electric power distribution system and its controllability. This paper proposes a new design based on a wound synchronous generator that overcomes this limitation by using different pole numbers for the windings to provide independent power supplies for both ship propulsion and ship services. In this novel approach, the two sets of windings physically share the same slots within a single machine frame but are fully electromagnetically decoupled. To investigate and validate this electromagnetic decoupling, the impact of load conditions such as resistive, resistive-inductive, and rectified DC loads are modelled and experimentally evaluated in detail. The results demonstrate that the novel dual wound generator operates as a fully decoupled machine, where the load change in one winding output does not impact the other winding, regardless of the load type. This unique ability to decouple the two outputs represents a significant innovation in the development of electric propulsion systems for transportation applications. This work therefore demonstrates the significant potential of the use of dual wound generators for applications in electric ships, electric aircraft, and heavy-duty vehicles, where independent power supplies are essential for efficient and reliable operation.

**INDEX TERMS** Dual wound synchronous generator, harmonic analysis, magnetic decoupling, dynamic loads, independent power supplies, ship propulsion power, ship services power.

## I. INTRODUCTION

Generator sets are widely employed in maritime integrated electric power systems to supply propulsion power and ship services as Fig. 1 (a), and offer two principal advantages:

i. The prime mover for the generators can be always operated in the high efficiency range to reduce the fuel consumption [1].

ii. The allocation of the prime movers and other auxiliary devices are more flexible [2].

Integrated power systems contribute to the reduction of greenhouse gas emissions, aligning with the increasingly stringent regulations [3]. With these advantages, they have proven to be highly successful in improving the performance of electric propulsion systems [4].

The introduction of dual generator machines presents further opportunities to enhance the systems. These machines consist of two sets of rotor and stator in a single frame, enabling more redundancy and more fault-tolerant capability in addition to footprint reduction and space saving benefits [5], [6].

In a further development a single stator and rotor can be equipped with two stator windings of the same pole number

The associate editor coordinating the review of this manuscript and approving it for publication was Kai Song.

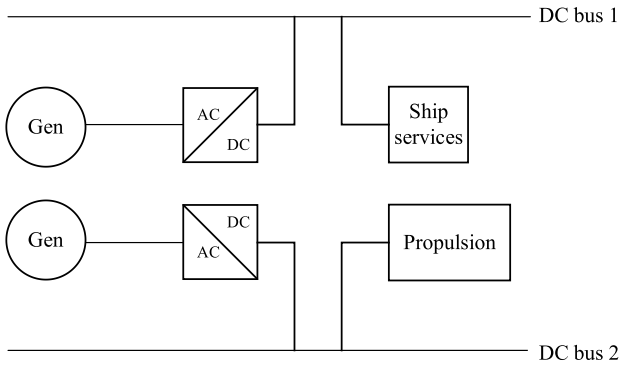


(a) Schematic architecture with two DC buses supplied by two conventional generators.

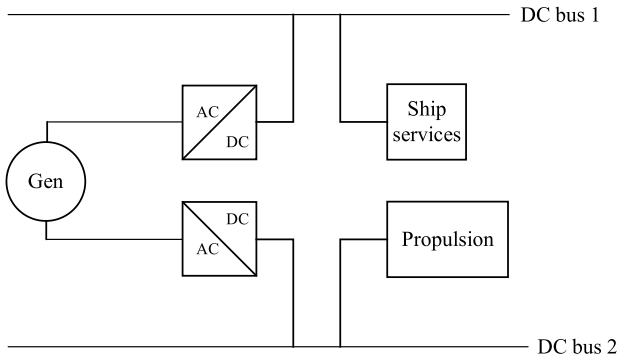


(b) Schematic architecture with two DC buses supplied by one dual wound generator.

**FIGURE 1. Architecture comparison for electric propulsion systems for ships.**

to provide dual outputs as shown in Fig.1 (b). Many of these machines [7], [8], [9] use conventional distributed double layer windings. This leads to magnetic coupling effects, which must be carefully considered and thoroughly investigated, particularly in maritime applications, where power supply demands can vary significantly due to multiple operating modes and conditions, and the impact of coupling becomes crucial [10], [11]. One concept proposed to power both port and starboard buses from a single generator with dual windings which offers redundancy and reduces the effects of prime mover light loading, but it inherently couples the two buses through the common generator [12]. The dynamic issues of galvanic and electro-mechanical coupling of power systems through a single dual wound generator are discussed [10].

A 20MW dual-wound generator has been designed for the electric power distribution system. Experimental results show that a load disturbance on one side of the generator can significantly affect the bus voltages on the other side, challenging the system's stability [13].

A further developed concept uses two concentrated tooth windings again of the same pole number arranged in alternate slots or sectors together with single permanent magnet excitation [14], [15], [16], [17]. These machines provide decoupling of the two outputs using the concentrated winding effect [18]. However, the machines inevitably have very large pole numbers which are unsuitable for maritime use and the outputs cannot be individually controlled.

An alternative system, the subject of this paper, uses two windings of different pole number designed so that no mutual harmonic coupling is present. The concept was first described in [19], [20], and [21] where the pole numbers used are in the normal range for maritime use and the outputs can be individually controlled. Reference [22] describes a dual output de-coupled machine using permanent magnet excitation. However, the full experimental validation of the machines is still lacking. The study in this paper begins with a comprehensive analysis of rotor field harmonics and winding factors for armature windings to mitigate the effects of magnetic coupling on the dynamic performance of the dual wound machine. Subsequently, a novel externally excited dual wound generator is proposed, designed to provide independent 2-pole and 6-pole outputs with 36-slot double layer windings in the stator, thereby ensuring complete decoupling between these winding sets. The theoretical analysis and design process aim to eliminate any magnetic coupling between the windings.

To validate the proposed theory and design, a 2D finite element (FE) model is employed to simulate the motor's performance and the extent of magnetic coupling under load changes. This FE model allows for a thorough examination of the machine's behavior in varying operating conditions. Detailed experimental tests are conducted, encompassing a range of conditions that reflect realistic operating modes, to validate the analytical analysis and simulation results. These experimental tests provide critical insights into the actual dynamic response and behavior of the dual wound generator, further confirming the effectiveness of the proposed design in achieving decoupling of the two winding outputs. The ultimate objective of this research is to develop a highly reliable and efficient dual wound generator, suitable for electric power distribution architecture and maritime integrated electric propulsion systems, where decoupling of the winding sets is of paramount importance for safe and stable operations.

## II. WINDING DESIGN

The winding redesign process is based on the existing wound synchronous generator available in the laboratory, which has 36 slots for the stator and 24 slots for the rotor. Normally, the diesel engine drives the shaft rotating at 60 Hz in ships. To match this rated speed, and also achieve a high winding factor and facilitate magnetic decoupling, the 2-pole and 6-pole configuration is selected. The magnetic couplings that must be eliminated in an externally excited 2-pole and 6-pole dual wound machine can be categorized as follows:

i The coupling between the 2-pole armature winding and the 6-pole armature winding.
ii The coupling between the 2-pole rotor winding and the 6-pole rotor winding.

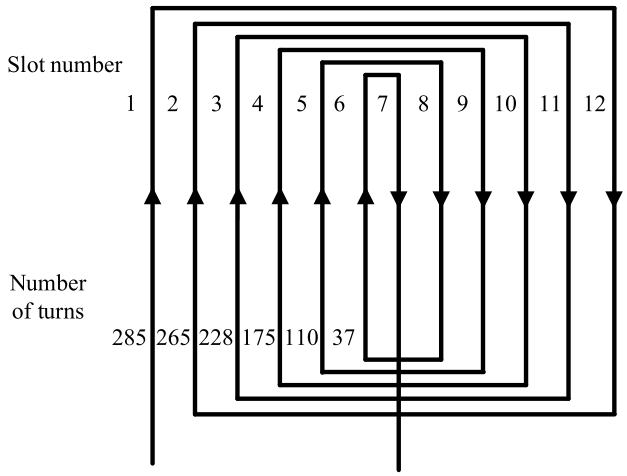


**FIGURE 2.** Diagram for one 2-pole concentric rotor coil set.

iii The coupling between the 2-pole armature winding and the 6-pole rotor winding.
iv The coupling between the 6-pole armature winding and the 2-pole rotor winding.

To reduce the harmonics of the rotor winding, concentric windings are utilized to realize a waveform of the field close to sinusoidal. The mechanical slot pitch angle is 15° for the rotor of 24 slots. To achieve different levels for forming a more sinusoidal waveform, the field strength required which is proportional to the number of turns in each slot for the 2-pole rotor winding can be expressed by (1). For the concentric winding, the field produced is obtained by superimposing the rectangular field distribution of individual coils, therefore, the number of turns required for each slot can be expressed as (2).

$$MMF_{sn} = MMF_{total} \sin \frac{n\pi}{12}, \quad n \in [1, 6] \tag{1}$$

$$\begin{cases} N_{s1} = N_{total} \sin \dfrac{\pi}{12} \\ N_{s2} = N_{total} \sin \dfrac{2\pi}{12} - N_{s1} \\ N_{s3} = N_{total} \sin \dfrac{3\pi}{12} - N_{s1} - N_{s2} \\ \cdots \\ N_{s6} = N_{total} \sin \dfrac{6\pi}{12} - N_{s1} - N_{s2} - \cdots - N_{s5} \end{cases} \tag{2}$$

Similarly, for the 6-pole rotor winding, the number of turns for each slot can be represented by (3).

$$\begin{cases} N_{s1} = N_{total} \sin \dfrac{\pi}{4} \\ N_{s2} = N_{total} \sin \dfrac{2\pi}{4} - N_{s1} \end{cases} \tag{3}$$

Based on (2) and (3), to achieve sinusoidal airgap field, the number of turns for each slot of two rotor winding sets are determined as shown in Fig. 2 and Fig. 3, respectively.

The magnetic field waveforms produced by two rotor windings are shown in Fig. 4. The amplitude of all the harmonics contained for each rotor field can be found in Table 1. It can be observed that there is no harmonics in common between the two rotor windings hence the magnetic coupling in between the rotor windings is insignificant.

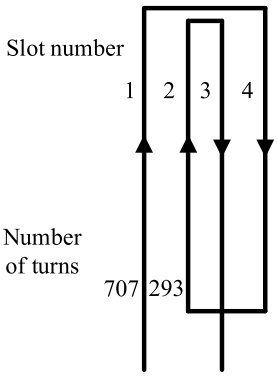


**FIGURE 3.** Diagram for one 6-pole concentric rotor coil set.

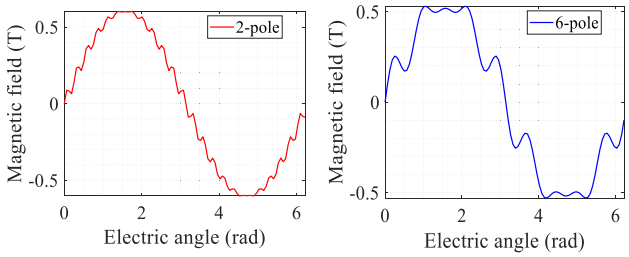


(a) 2-pole rotor field (b) 6-pole rotor field

**FIGURE 4.** Magnetic field waveform for 2-pole and 6-pole rotor winding sets based on analytical calculation.

**TABLE 1.** Magnetic field harmonics for 2-pole and 6-pole rotor windings.

| Harmonics order | Magnetic field (T) | |
|---|---|---|
| | 2-p | 6-p |
| 1 | 0.603 | 0 |
| 3 | 0 | 0.536 |
| 21 | 0 | 0.077 |
| 23 | 0.026 | 0 |
| 25 | 0.024 | 0 |
| 27 | 0 | 0.060 |

Considering the armature windings, if a slot in a machine at $\theta_s$ contains $N_s$ conductors, the resulting conductor distribution can be described as (4) assuming that the slot conductors form a point conductor [23], [24]. For the phase $a$ that has $S$ slots, the resultant conductor distribution for the harmonic order of $p$ can be expressed as (5).

$$\overline{N}_p = \frac{1}{\pi} N_s e^{-jp\theta_s} \tag{4}$$

$$\overline{N}_{pa} = \frac{1}{\pi} \sum_{s=1}^{S} N_{sa} e^{-jp\theta_{sa}} = N_{pa} e^{j\phi_{pa}} \tag{5}$$

The winding distributions for three phase windings can be represented by positive phase sequence (PPS), negative phase

sequence (NPS) and zero phase sequence (ZPS). The position and amplitude of the first of the three-phase coil set for each harmonic is given as (6)-(8).

$$n_{pp} = \frac{1}{3}[N_{pa}e^{j\phi_{pa}} + N_{pb}e^{j(\phi_{pb}+\frac{2}{3}\pi)} + N_{pc}e^{j(\phi_{pc}-\frac{2}{3}\pi)}] \quad (6)$$

$$n_{np} = \frac{1}{3}[N_{pa}e^{j\phi_{pa}} + N_{pb}e^{j(\phi_{pb}-\frac{2}{3}\pi)} + N_{pc}e^{j(\phi_{pc}+\frac{2}{3}\pi)}] \quad (7)$$

$$n_{zp} = \frac{1}{3}[N_{pa}e^{j\phi_{pa}} + N_{pb}e^{j\phi_{pb}} + N_{pc}e^{j\phi_{pc}}] \quad (8)$$

**TABLE 2.** Winding factors for 2-pole and 6-pole full-pitched armatures.

| Harmonics order | PPS | | NPS | | ZPS | |
|---|---|---|---|---|---|---|
| | 2-p | 6-p | 2-p | 6-p | 2-p | 6-p |
| 1 | 0.956 | 0 | 0 | 0 | 0 | 0 |
| 3 | 0 | 0.966 | 0 | 0 | 0.644 | 0 |
| 5 | 0 | 0 | 0.197 | 0 | 0 | 0 |
| 7 | 0.145 | 0 | 0 | 0 | 0 | 0 |
| 9 | 0 | 0 | 0 | 0 | 0.236 | 0.707 |
| 11 | 0 | 0 | 0.102 | 0 | 0 | 0 |
| 13 | 0.092 | 0 | 0 | 0 | 0 | 0 |
| 15 | 0 | 0 | 0 | 0.259 | 0.173 | 0 |
| 17 | 0 | 0 | 0.084 | 0 | 0 | 0 |
| 19 | 0.084 | 0 | 0 | 0 | 0 | 0 |
| 21 | 0 | 0.259 | 0 | 0 | 0.173 | 0 |
| 23 | 0 | 0 | 0.092 | 0 | 0 | 0 |
| 25 | 0.102 | 0 | 0 | 0 | 0 | 0 |
| 27 | 0 | 0 | 0 | 0 | 0.24 | 0.707 |

Based on the above, the winding factors for 2-pole and 6-pole 36-slot full-pitch winding sets can be expressed as (9) and (10). It is worthwhile to mention that the winding factor is equal to the distribution factor in this case when full-pitch windings are considered.

$$k_{F2wp} = k_{F2dp} = \left|\frac{\sin\left(\frac{\pi p}{6}\right)}{6\sin\left(\frac{p\pi}{36}\right)}\right| \quad (9)$$

$$k_{F6wp} = k_{F6dp} = \left|\frac{\sin\left(\frac{\pi p}{18}\right)}{2\sin\left(\frac{p\pi}{36}\right)}\right| \quad (10)$$

The winding factors for 2-pole armature and 6-pole armature windings are shown in Table 2. It can be seen that the PPS and NPS have no coupling between 2-pole armature and 6-pole armature but have harmonics of the same order in ZPS which would introduce magnetic coupling between two armature sets.

To mitigate the magnetic coupling, double layer windings are used for both 2-pole and 6-pole armature windings. For 2-pole winding, the top and bottom layers are in the same position using fully pitched coils while offsetting the bottom layer by 1/3 pole pitch results in 2/3 short-pitch windings. For the 6-pole winding, offsetting the bottom layer by 1/6 coil pitch results in 5/6 short-pitch windings. The effect of the offset of the layers can be described by (11). It follows that the conductor distribution $\overline{N}_{pa}$ for the $p^{th}$ harmonic of a phase winding is multiplied by $cos(p\alpha/2)$ when a $\alpha$ offset is applied. Therefore, the winding factors for 2-pole armature and 6-pole armature are modified as shown in (12) and (13).

$$\overline{N}_{pao} = N_{pa}(1+e^{-jp\alpha}) = N_{pa}2e^{\frac{jp\alpha}{2}}\cos\frac{p\alpha}{2} \quad (11)$$

$$k_{S2wp} = \left|\frac{\sin\left(\frac{\pi p}{6}\right)}{6\sin\left(\frac{p\pi}{36}\right)}\cos\frac{p\pi}{6}\right| \quad (12)$$

$$k_{S6wp} = \left|\frac{\sin\left(\frac{\pi p}{18}\right)}{2\sin\left(\frac{p\pi}{36}\right)}\cos\frac{p\pi}{36}\right| \quad (13)$$

**TABLE 3.** Winding factors for 2-pole and 6-pole short-pitched double layer armatures.

| Harmonics order | PPS | | NPS | | ZPS | |
|---|---|---|---|---|---|---|
| | 2-p | 6-p | 2-p | 6-p | 2-p | 6-p |
| 1 | 0.828 | 0 | 0 | 0 | 0 | 0 |
| 3 | 0 | 0.933 | 0 | 0 | 0 | 0 |
| 5 | 0 | 0 | 0.171 | 0 | 0 | 0 |
| 7 | 0.126 | 0 | 0 | 0 | 0 | 0 |
| 9 | 0 | 0 | 0 | 0 | 0 | 0.5 |
| 11 | 0 | 0 | 0.088 | 0 | 0 | 0 |
| 13 | 0.080 | 0 | 0 | 0 | 0 | 0 |
| 15 | 0 | 0 | 0 | 0.067 | 0 | 0 |
| 17 | 0 | 0 | 0.072 | 0 | 0 | 0 |
| 19 | 0.072 | 0 | 0 | 0 | 0 | 0 |
| 21 | 0 | 0.067 | 0 | 0 | 0 | 0 |
| 23 | 0 | 0 | 0.080 | 0 | 0 | 0 |
| 25 | 0.088 | 0 | 0 | 0 | 0 | 0 |
| 27 | 0 | 0 | 0 | 0 | 0 | 0.5 |

As a result, the winding factors for two short-pitched armature windings are shown in Table 3. It shows that the harmonics of zero phase sequence for 2-pole winding are completely removed and there are now no harmonics of the same order in the 2-pole winding and 6-pole winding, which means the magnetic coupling has been eliminated. The winding diagram for 2-pole armature and 6-pole armature are shown in Fig. 5. Moreover, after the offsetting, the 6-pole rotor winding has eliminated the impacts on the 2-pole armature winding as shown in Table 1 and Table 2.

## III. FINITE ELEMENT MODELING

The primary focus of this paper is to eliminate the coupling effects when a dynamic load change occurs. This section presents the simulation results when a resistive and inductive load are applied separately to both the 2-pole and 6-pole outputs. The 2D model is built as shown in Fig. 6 based on the geometry of the existing generator using extra fine mesh in the simulation.

Firstly, the effect of pure resistive load change was investigated. By adding external three-phase 60 Ω resistive load for the 2-pole output and 80 Ω for the 6-pole output, and defining the time they are switched in, the dynamic load conditions can be simulated.

Fig. 7 shows the simulation results when a load change occurs in the 2-pole armature winding when the 6-pole armature winding is loaded at rated output. It can be seen that at the

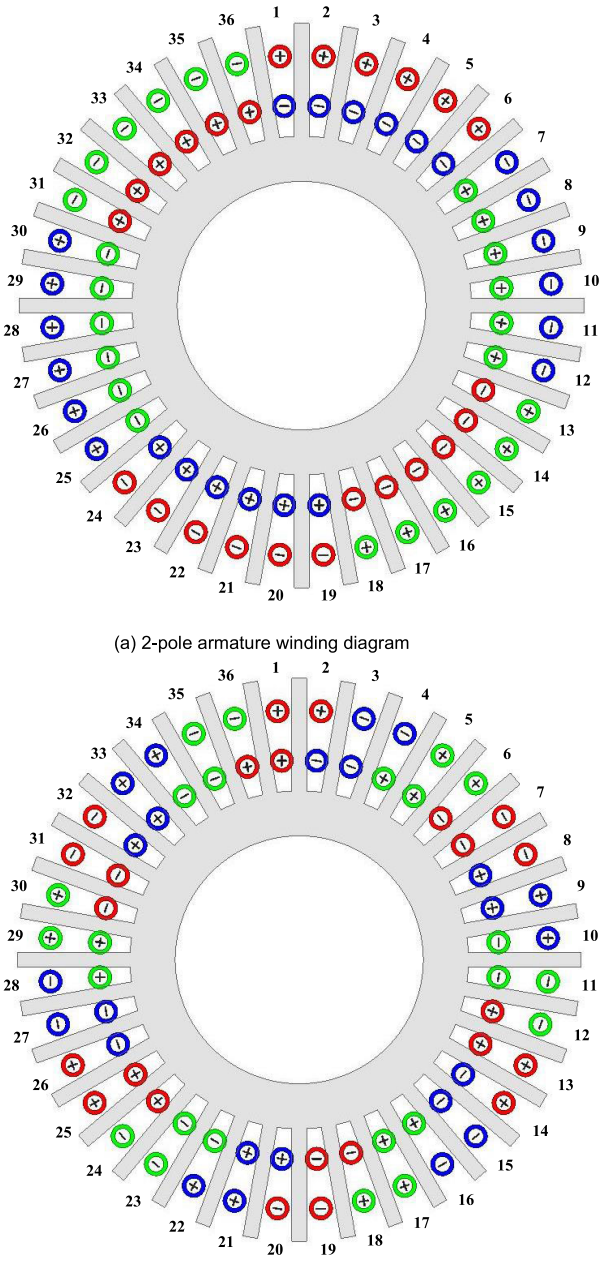

(a) 2-pole armature winding diagram

(b) 6-pole armature winding diagram

**FIGURE 5.** Winding diagram for 2-pole and 6-pole winding sets.

start the resistive load is switched on and the 2-pole winding current increases from zero to the rated peak current of 2.5 A. The terminal voltage for the 2-pole output remains at the peak value of 154 V with only a short disturbance. Moreover, there is no disturbance observed on both the current and the voltage outputs for the 6-pole armature winding which maintains the voltage of 129 V and the current of 1.6 A.

Fig. 8 shows the simulation results when applying a dynamic resistive load change for 6-pole armature winding while 2-pole armature winding is loaded at rated output. It can be observed that when the load is changed at the start for

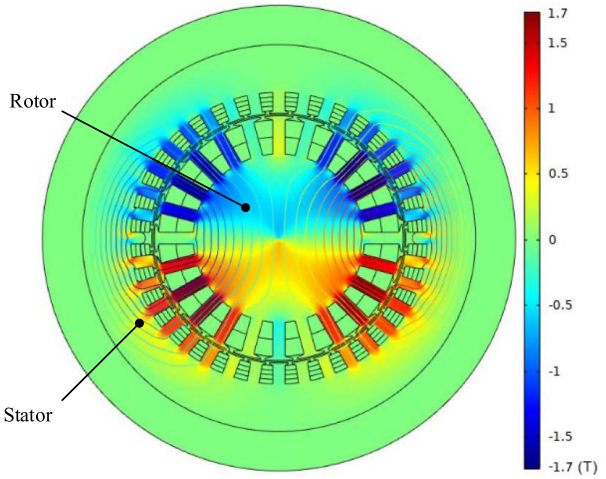


**FIGURE 6.** 2D FE model for the dual wound machine.

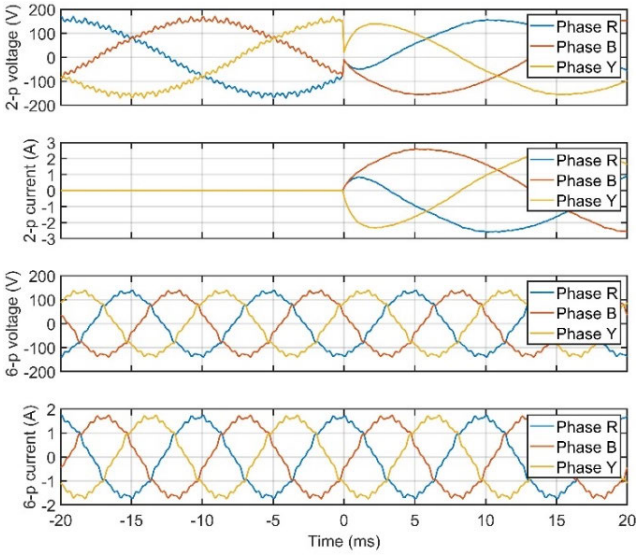


**FIGURE 7.** Simulation results for 2-pole and 6-pole outputs when resistive load dynamic change occurs in 2-pole windings.

6-pole winding, there is no impact on either the voltage or the current from the 2-pole winding.

All these results show that there is no magnetic coupling between 2-pole armature windings and 6-pole armature windings when a pure resistive load change happens in the system.

To simulate more realistic operating conditions for electric ships, a resistive-inductive (RL) load was applied to the dual wound generator. The simulation assumes the 6-pole output operating with a three-phase 80 Ω load, while the 2-pole output load current changes. At time zero, a three-phase load consisting of 60 Ω resistors and 100 mH inductors was connected to the 2-pole output winding. The simulation results, depicted in Fig. 9, show a transient fluctuation in the 2-pole output at the moment of load connection. However, the output quickly returns to normal operation, achieving a voltage of 150 V and a current of 2.3 A. Notably, a comparison of

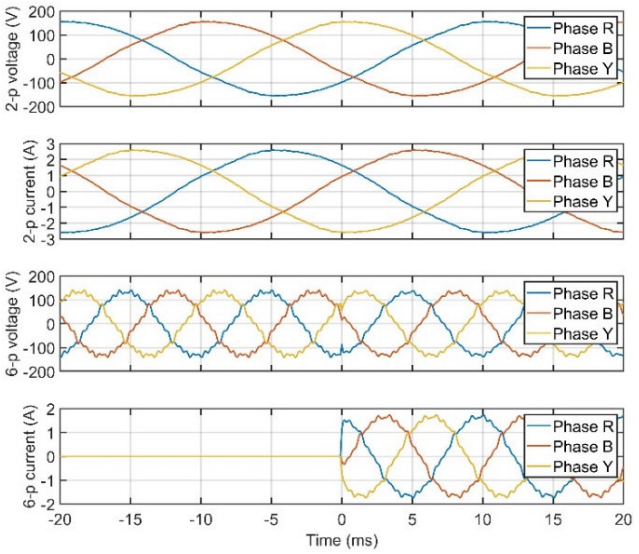


**FIGURE 8.** Simulation results for 2-pole and 6-pole outputs when dynamic resistive load change occurs in 6-pole windings.

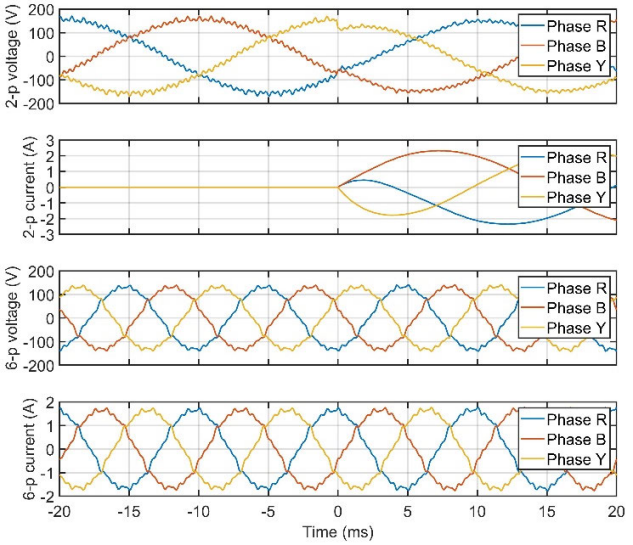


**FIGURE 9.** Simulation results for 2-pole and 6-pole outputs when dynamic resistive-inductive load change occurs in 2-pole windings.

the current waveforms between the cases of pure resistive load (Fig. 7) and resistive-inductive load (Fig. 9) shows a difference in the peak current timing. With pure resistive load, the current peaks at 5 milliseconds, while with the resistive-inductive load, the current peaks at 7 milliseconds, due to the additional inductance introduced into the windings.

The 6-pole output exhibited no observable effects from the 2-pole windings. It maintains stable output conditions for both voltage and current. These simulation results verify the effective decoupling of the dual wound generator's windings, as the 6-pole output remained isolated from the load variations in the 2-pole output even under dynamic resistive-inductive load conditions. Furthermore, the simulation results for the effects of dynamic resistive-inductive load change on the 6-pole output, shown in Fig. 8, confirms the absence of magnetic coupling in this scenario. The dual wound generator demonstrated its capability to handle resistive-inductive loads without compromising the independence of its output windings, further enhancing its potential suitability for electric ships and similar applications.

## IV. EXPERIMENTAL RESULTS AND DISCUSSIONS

### A. TEST PLATFORM CONFIGURATION

The prototype of the designed dual wound generator has been built. Following the redesign requirements to validate the dynamic magnetic decoupling performance, the windings were rewound based on the new winding design using the existing generator. The specifications of the designed dual wound generator are listed in Table 4. All the components required to conduct the experiments are depicted in Fig. 11 and the description of each component is listed in Table 5.

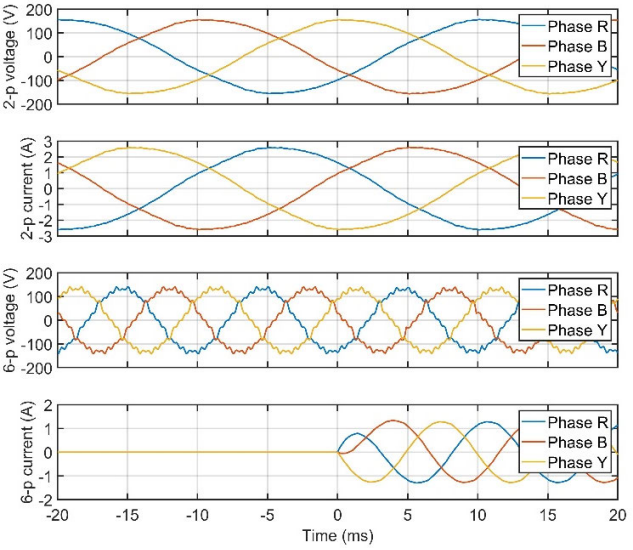


**FIGURE 10.** Simulation results for 2-pole and 6-pole outputs when dynamic resistive-inductive load change occurs in 6-pole windings.

### B. ROTOR FIELD DYNAMIC CHANGE TEST

To investigate the potential impact of changing one of the rotor excitation currents on the other output, an experimental test was conducted on the dual wound generator by increasing the rotor excitation current. During this test, the two stator windings supplied their rated resistances, that is, 60 Ω for the 2-pole winding and 80 Ω for the 6-pole winding.

As depicted in Fig. 12, a resistor is connected in series in the rotor excitation circuit to maintain a low initial rotor current. The resistor is then short-circuited by the circuit breaker to increase the rotor excitation current to 1 A. Notably, the external resistor is set to have the same resistance value as the

**TABLE 4.** Specification of the dual wound generator.

| Specification | Stator | Rotor |
|---|---|---|
| Number of slots | 36 | 24 |
| Axial length (mm) | 123.6 | 139.5 |
| Slot opening (mm) | 2.7 | 3.5 |
| Stator outer diameter (mm) | 295 | |
| Stator inner diameter (mm) | 190.5 | |
| Rotor outer diameter (mm) | 186.5 | |
| Airgap (mm) | 2 | |
| 2-pole Rotor winding resistance (Ω) | 179.6 | |
| 6-pole Rotor winding resistance (Ω) | 418.9 | |
| Rated excitation current for both 2-pole field and 6-pole field (A) | 1 | |

**TABLE 5.** Description of the component used on the test bench.

| Component | Description |
|---|---|
| Externally excited DC motor | Prime mover<br>Rated power: 5 kW<br>Rated rotating speed: 3000 rpm |
| LAB/SMS630 | DC power supply for the field current of the DC motor |
| LAB/SMS5300 | DC power supply for the armature current of the DC motor |
| Dual wound generator | Machine under test |
| EA-PS 8360-15 | DC power supply for the 2-pole field excitation of the dual wound generator |
| LAB-SMP11200 | DC power supply for the 6-pole field excitation of the dual wound generator |
| Three-phase resistor | 60 Ω for 2-pole output and 80 Ω for 6-pole output for realizing the dynamic resistive load change through a switch |
| Three-phase inductor | 100mH for both 2-pole output and 6-pole output for realizing the dynamic inductive load change through a switch |
| Oscilloscope | Monitoring the output voltage and current waveform from the dual wound generator |
| Tachometer | Measurement of the rotating speed |

corresponding rotor winding, ensuring that the rotor current is effectively doubled when the circuit breaker is turned on.

This setup allows a controlled examination of how changes in one rotor excitation current may influence the other output and evaluates the effectiveness of the decoupled rotor winding design.

Fig. 13 presents the dynamic changes in the 2-pole and 6-pole stator voltages when the 2-pole rotor current is increased from 0.5 A to 1 A by the circuit breaker.

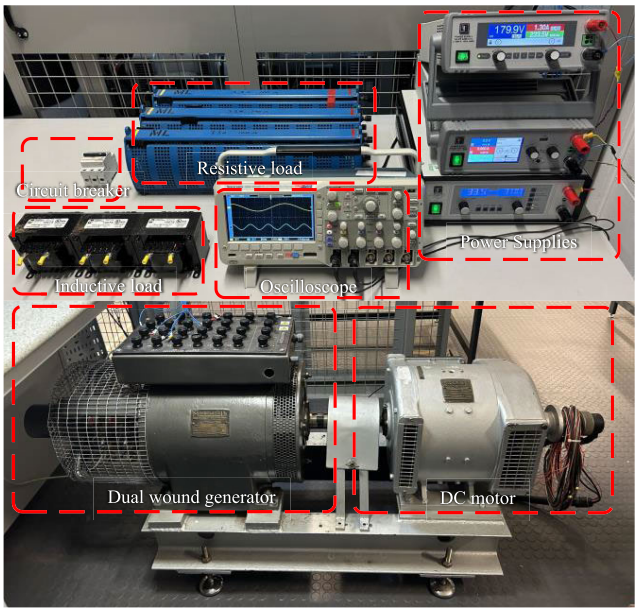


**FIGURE 11.** Experimental test platform.

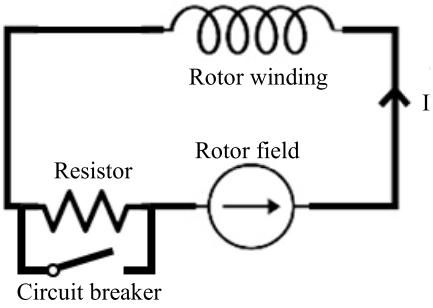


**FIGURE 12.** Rotor field dynamic change test circuit.

As anticipated, the 2-pole stator voltage rises with the increase in the 2-pole rotor excitation current. However, it is important to note that due to the constant input power of the DC motor, this results in a reduction in the rotating speed of the prime mover.

It is observed that at 1 A rotor current, the peak voltage of the 2-pole stator is lower than twice the value at 0.5 A rotor current, primarily due to the rotational speed drop. Additionally, the 6-pole voltage, as depicted in Fig. 13, exhibits a slight decrease with the increasing 2-pole rotor excitation current, which can also be attributed to the reduction in rotating speed.

Notably, despite the sudden change in the 2-pole field, no disturbances or unexpected instantaneous output fluctuations are introduced on the 6-pole output. This observation reinforces the effectiveness of the decoupled winding design of the dual wound generator in maintaining the stability of the system during changing of the 2-pole rotor excitation current.

Fig. 14 displays the experimental test results when increasing the 6-pole rotor current from 0.6 A to 1 A by the circuit breaker. As anticipated, the 6-pole stator output voltage exhibits an increase with the rise in the 6-pole rotor excitation

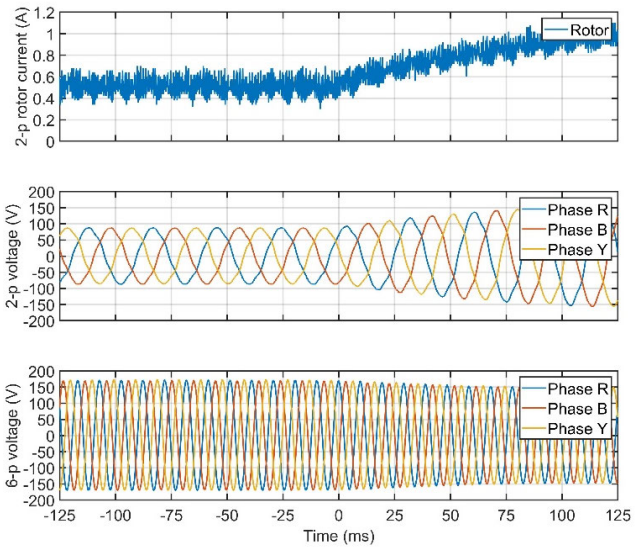


**FIGURE 13.** Results from 2-pole rotor current dynamic change test.

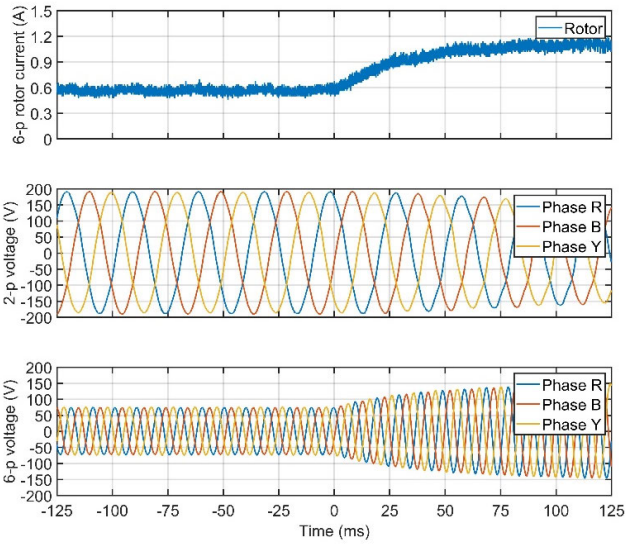


**FIGURE 14.** Results from 6-pole rotor current dynamic change test.

current. In the same way as the effects observed with changes in the 2-pole rotor current, the rotating speed of the prime mover experiences a slight decrease due to the increase in the 6-pole rotor current. Consequently, the 2-pole stator output voltage also decreases.

An encouraging finding from these experiments is the absence of disturbances and waveform distortions arising from increased harmonics, which could have resulted from magnetic coupling between the 6-pole rotor and the 2-pole output. As such, it can be concluded that the rotor current solely affects the corresponding stator winding, and there is no evidence of undesired magnetic coupling between the two rotors and the other outputs.

These results verify the effectiveness of the decoupled winding design of the dual wound generator, as it successfully isolates the effects of rotor current changes and ensures minimal interference on the 2-pole and 6-pole outputs.

### C. RESISTIVE LOAD DYNAMIC CHANGE TEST

In an electric ship propulsion system, the variations in propulsion and service power demand during different operations necessitate the assurance that changes in load on one output does not affect the other output. Fig. 15 and Fig. 16 present the results of the dynamic resistive load change tests.

The dynamic load test for the 2-pole output starts by operating it under a no-load condition. Subsequently, the rated 3-phase resistive load is introduced to the 2-pole output, while the 6-pole output remains at its rated load condition. The test results for the 2-pole output dynamic load are illustrated in Fig. 15. Initially, the 2-pole stator current starts from zero and increases to its rated level. The 2-pole stator voltage shows transient changes when the load is connected and returns to the rated 3-phase sinusoidal waveform. In contrast, the 6-pole stator voltage remains stable and unaffected throughout the test.

Following the same testing process as the 2-pole dynamic load test, the dynamic load test results for the 6-pole resistive load are depicted in Fig. 16. At the beginning of the test, the 6-pole stator has no current as it operates under a no-load condition. Subsequently, the current increases to its rated value when the load is connected. During the switching process, slight voltage ripples are observed on the 6-pole stator voltage; however, the waveform returns to its normal voltage in a short time.

Based on the experimental test results for the resistive load dynamic change in this section, it is evident that changes in the resistive load on the 2-pole output have no impact on the 6-pole output, and vice versa. This outcome reaffirms the effectiveness of the dual wound generator's design, demonstrating its ability to maintain isolated operation of the two outputs, ensuring minimal interference between them.

### D. RL LOAD DYNAMIC CHANGE TEST

The successful decoupling of the two windings during the resistive load dynamic change test encourages the investigation of a more intricate operational scenario, specifically the inductive load test.

In the dynamic resistive-inductive load test, each phase of the 2-pole output is subjected to a load consisting of a 60 Ω resistance and a 100 mH inductance connected in series. Similarly, the corresponding values for the 6-pole output are an 80 Ω resistance and a 100 mH inductance. The testing procedure mirrors that of the resistive load dynamic test, wherein the output is initially operated under a no-load condition and subsequently loaded with the specified resistive and inductive loads. During this testing process for one output, the

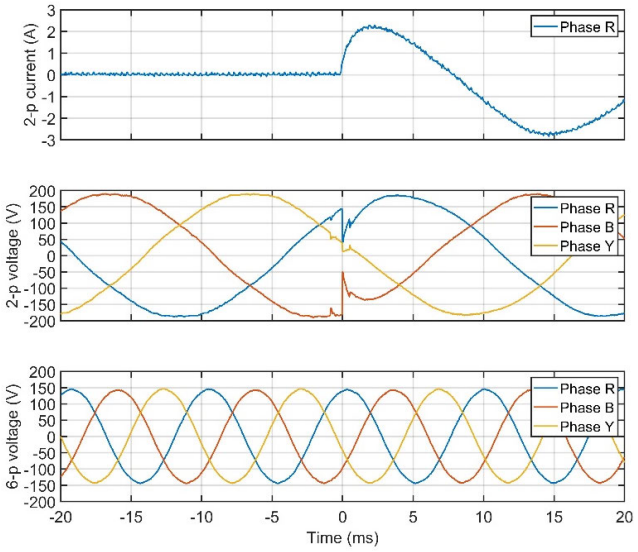


**FIGURE 15.** Result from 2-pole resistive load dynamic change test.

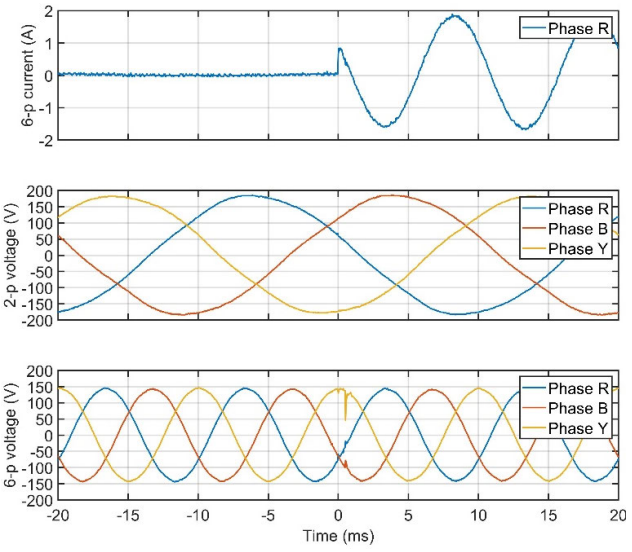


**FIGURE 16.** Results from 6-pole resistive load dynamic change test.

other output is maintained at its rated 3-phase resistive load condition.

Fig. 17 displays the results of the 2-pole output resistive and inductive load dynamic change test. As the load is connected, the 2-pole stator current starts to increase; however, the first peak value does not reach the rated peak current due to the presence of the inductive load. It is noteworthy that the 2-pole stator voltage is affected upon the switching of the 2-pole loads in the circuit, while the 6-pole voltage remains consistently stable, thereby indicating the successful decoupling of the two winding outputs under the inductive load condition.

Fig. 18 exhibits the results of the resistive-inductive load dynamic change test for the 6-pole winding output. In the same way the 2-pole output test, the load switching solely

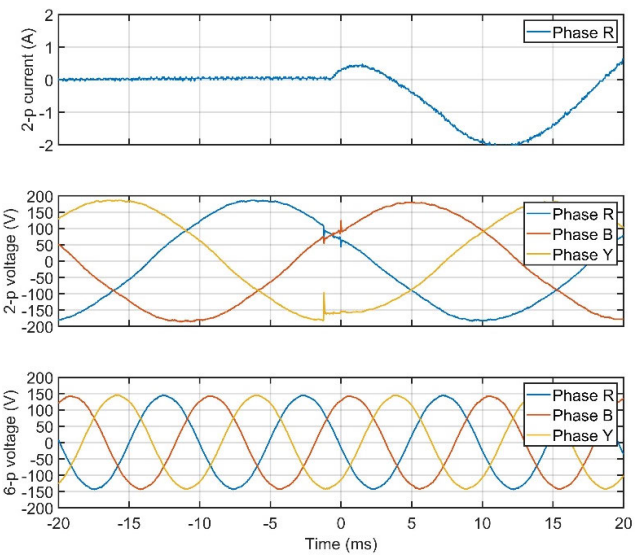


**FIGURE 17.** Results from 2-pole resistive-inductive load dynamic change test.

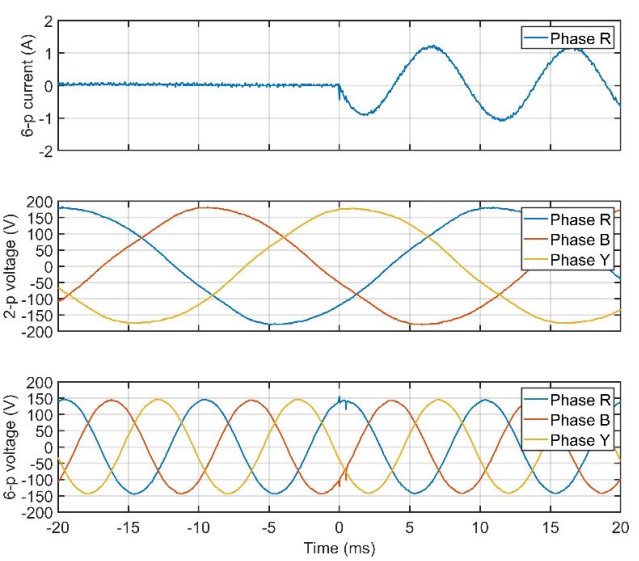


**FIGURE 18.** Results from 6-pole resistive-inductive load dynamic change test.

affects the 6-pole voltage, without any impact on the 2-pole output. These results further substantiate the independence of the two outputs under a more complex load condition during dynamic operation.

### *E. RECTIFIED DC LOAD DYNAMIC CHANGE TEST*

In this section, the performance of the dual wound generator under a rectified DC load test is investigated, this is important for electric propulsion ship systems employing DC distribution networks. The test involves using a full-bridge rectifier (VS-36MT120) to establish a DC bus from both the 2-pole and 6-pole stator outputs, with resistive loads connected to verify the decoupling of the two winding outputs under dynamic rectifier conditions.

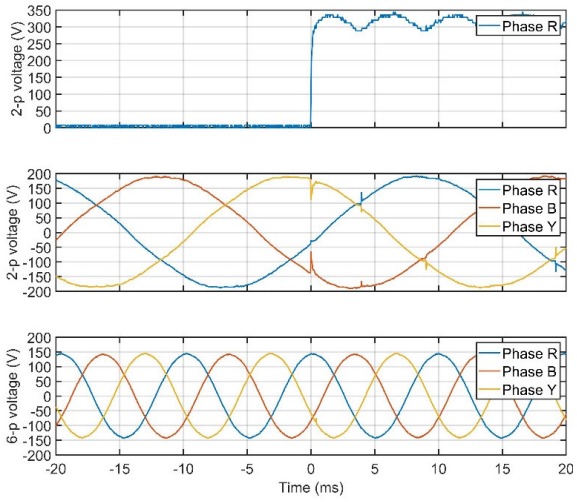


**FIGURE 19.** Results from 2-pole rectified DC load dynamic change test.

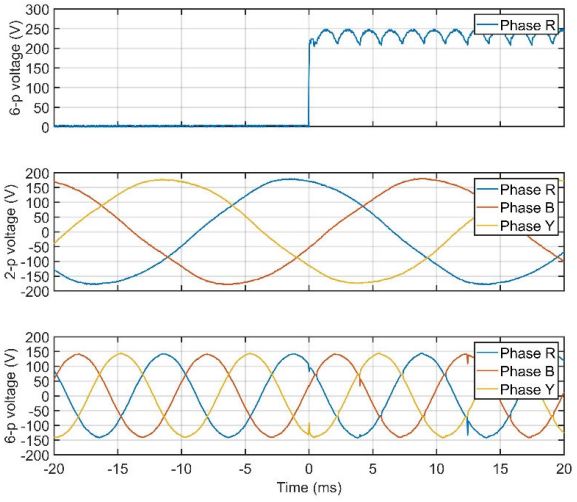


**FIGURE 20.** Results from 6-pole rectified DC load dynamic change test.

For this test, DC resistive loads of 1000 Ω and 500 Ω are applied to the 2-pole and 6-pole rectifier outputs, respectively. The winding output under examination starts in a no-load condition and subsequently the DC resistive load is connected into the DC bus. During the test, the other output is maintained at its rated 3-phase loaded condition.

Fig. 19 illustrates the results of the 2-pole rectified load dynamic change test. The 2-pole stator rectified DC voltage increases from zero to 320 Vdc upon switching. At each switching point, slight ripples appear on the primary side of the 2-pole stator voltage, while there is minimal effect on the 6-pole stator.

Similarly, Fig. 20 presents the rectified DC load dynamic change test results for the 6-pole winding output. The rectified voltage for the 6-pole output is set at 230 Vdc. Upon switching the 6-pole DC resistive load to the circuit, there is no noticeable impact on the 2-pole output. However, the 6-pole stator voltage exhibits some ripple content at each rectifier switching point.

The dynamic test on the rectifier circuit demonstrates the dual wound generator is capable of providing an onboard DC bus using one of its stator windings without affecting the other winding. These results further validate the effective decoupling of the two winding outputs under dynamic rectifier conditions, enhancing the reliability and versatility of the dual wound generator in electric propulsion systems.

## V. CONCLUSION

This paper investigates the performance of a novel dual-wound generator designed and constructed to handle a range of operating load conditions, providing a practical electric propulsion system for shipping applications. It addresses the common challenge of magnetic coupling between the two outputs of the dual-wound generator. The new design is proposed based on a wound synchronous generator that provides independent power supplies for ship propulsion and ship services, thereby avoiding magnetic coupling between the outputs. In this novel approach, the two sets of windings physically share the same slots within a single machine frame but are electromagnetically fully decoupled.

The arrangement of the 2-pole and 6-pole windings was analyzed in detail to eliminate electromagnetic coupling and achieve harmonic decoupling through the winding design. The aim was to ensure the two winding outputs function independently, enabling the generator to provide independent power supplies for electric propulsion and ship services.

Two-dimensional finite element analysis was utilized to validate the decoupling performance of the dual wound generator under the dynamic change of resistive and inductive loads. The experimental tests conducted on the dual wound generator prototype provide evidence that the two winding outputs, including the end-windings, are completely decoupled under different load conditions and when subjected to different forms of dynamic load changes. As a result, the 2-pole and 6-pole windings can independently generate power supplies without affecting each other or the overall system. This capability ensures the provision of independent and reliable power sources for both electric propulsion and ship service applications.

In summary, our detailed modelling and experimental results demonstrate that the novel dual wound generator operates as a fully decoupled machine and the unique ability to decouple the two outputs represents a significant innovation in the development of electric propulsion systems for shipping applications. The implications of this paper also extend beyond electric propulsion ship systems and have potential applications in other transport, including electric aircraft, railroads, buses, and heavy-duty trucks. The demonstrated success of the dual wound generator prototype highlights its versatility and effectiveness in addressing the challenges posed by different dynamic load conditions in modern electric power systems.

## REFERENCES


[1] J. S. Thongam, M. Tarbouchi, A. F. Okou, D. Bouchard, and R. Beguenane, "All-electric ships—A review of the present state of the art," in *Proc. 8th Int. Conf. Exhib. Ecol. Vehicles Renew. Energies (EVER)*, Mar. 2013, pp. 1–8, doi: 10.1109/EVER.2013.6521626.

[2] S. Kanerva and J.-F. Hansen, "State of the art in electric propulsion—Viewpoint on redundancy," in *Proc. IEEE Electric Ship Technol. Symp.*, Apr. 2009, pp. 499–504, doi: 10.1109/ESTS.2009.4906558.

[3] T. W. P. Smith. (2015). *Third IMO Greenhouse Gas Study 2014*. Accessed: Jul. 17, 2023. [Online]. Available: https://research.manchester.ac.uk/en/publications/third-imo-greenhouse-gas-study-2014

[4] J. F. Hansen, F. Wendt, J. Nowak, K. Hansen, and K. Stenersen, "Integrated power and automations system for enhanced performance of DP class drilling vessels," in *Proc. DP Conf.*, 2013, pp. 1–14.

[5] A. M. El-Refaie, "Fault-tolerant permanent magnet machines: A review," *IET Electr. Power Appl.*, vol. 5, no. 1, p. 59, Jan. 2011, doi: 10.1049/iet-epa.2009.0117.

[6] X. Jiang, W. Huang, R. Cao, Z. Hao, and W. Jiang, "Electric drive system of dual-winding fault-tolerant permanent-magnet motor for aerospace applications," *IEEE Trans. Ind. Electron.*, vol. 62, no. 12, pp. 7322–7330, Dec. 2015, doi: 10.1109/TIE.2015.2454483.

[7] P. L. Alger, E. H. Freiburghouse, and D. D. Chase, "Double windings for turbine alternators," *Trans. Amer. Inst. Electr. Eng.*, vol. 49, no. 1, pp. 226–244, Jan. 1930, doi: 10.1109/T-AIEE.1930.5055483.

[8] E. F. Fuchs and L. T. Rosenberg, "Analysis of an alternator with two displaced stator windings," *IEEE Trans. Power App. Syst.*, vol. PAS-93, no. 6, pp. 1776–1786, Nov. 1974, doi: 10.1109/TPAS.1974.293829.

[9] D. Hadiouche, H. Razik, and A. Rezzoug, "On the modeling and design of dual-stator windings to minimize circulating harmonic currents for VSI fed AC machines," *IEEE Trans. Ind. Appl.*, vol. 40, no. 2, pp. 506–515, Apr. 2004, doi: 10.1109/TIA.2004.824511.

[10] L. J. Rashkin, J. C. Neely, S. F. Glover, T. J. McCoy, and S. D. Pekarek, "Dynamic considerations of power system coupling through dual-wound generators," in *Proc. IEEE Electr. Ship Technol. Symp. (ESTS)*, Aug. 2017, pp. 493–500, doi: 10.1109/ESTS.2017.8069327.

[11] T. Donnelly, L. Rashkin, and M. Cook, "Performance evaluation of a dual wound generator for naval power system applications," in *Proc. IEEE Transp. Electrific. Conf. Expo (ITEC)*, Jun. 2023, pp. 1–7, doi: 10.1109/ITEC55900.2023.10187029.

[12] N. Doerry and J. Amy, "The Road to MVDC," in *Proc. ASNE Intell. Ships Symp.*, 2015, pp. 68–73.

[13] L. J. Rashkin, J. C. Neely, S. F. Glover, T. J. McCoy, and N. Doerry, "Dynamic response evaluation of a 20 MW scale dual wound machine based power system," Sandia Nat. Lab., Albuquerque, NM, USA, Tech. Rep., SAND2018-2720C, 2018.

[14] N. Velly, N. Takorabet, F. Meibody-Tabar, P. Y. Liegeois, F. Nierlich, F. N. Leynaert, and G. Humbert, "Double channel PM motor for avionic applications: Impact of winding topologies," in *Proc. IEEE Energy Convers. Congr. Expo.*, Sep. 2009, pp. 2387–2394, doi: 10.1109/ECCE.2009.5316340.

[15] E. Mese, M. Tezcan, M. Ayaz, Y. Yasa, and K. Yilmaz, "Design considerations for dual winding permanent magnet synchronous machines," in *Proc. IEEE Energy Convers. Congr. Expo. (ECCE)*, Sep. 2012, pp. 1894–1901, doi: 10.1109/ECCE.2012.6342581.

[16] M. Ayaz, M. Tezcan, K. Yilmaz, and E. Mese, "Magnetic coupling effect of a PM synchronous machine having concentrated windings," in *Proc. 6th IET Int. Conf. Power Electron., Mach. Drives (PEMD )*, Mar. 2012, pp. 1–6, doi: 10.1049/cp.2012.0305.

[17] T. Yazdan, M. Humza, and H.-W. Cho, "Three-phase dual-winding multitasked PMSM machine using double layer concentrated winding for HEV application," *IEEE Access*, vol. 11, pp. 36682–36691, 2023, doi: 10.1109/ACCESS.2023.3264568.

[18] A. M. El-Refaie, T. M. Jahns, and D. W. Novotny, "Analysis of surface permanent magnet machines with fractional-slot concentrated windings," *IEEE Trans. Energy Convers.*, vol. 21, no. 1, pp. 34–43, Mar. 2006, doi: 10.1109/TEC.2005.858094.

[19] C. G. Hodge and J. F. Eastham, "Dual wound machines for electric ship power systems," in *Proc. IEEE Electr. Ship Technol. Symp. (ESTS)*, Jun. 2015, pp. 62–67, doi: 10.1109/ESTS.2015.7157862.

[20] B. Yin, X. Pei, X. Zeng, F. Eastham, C. Hodge, and O. Simmonds, "Design and analysis of dual wound machine for electric ships," in *Proc. Int. Conf. Electr. Mach. (ICEM)*, vol. 1. Gothenburg, Sweden: IEEE, Aug. 2020, pp. 104–110, doi: 10.1109/ICEM49940.2020.9270913.

[21] C. G. Hodge, F. Eastham, and A. C. Smith, "The harmonic analysis of machine excitation," in *Proc. Int. Nav. Eng. Conf. (INEC)*, Edinburgh, U.K., 2012, pp. 15–17.

[22] J. F. Eastham, B. Yin, X. Zeng, C. Hodge, and X. Pei, "Permanent magnet excitation of a two and four pole pair dual wound machine," in *Proc. NEC*, 2022, pp. 1–12, doi: 10.24868/10662.

[23] J. F. Eastham and C. G. Hodge, "The harmonics analysis of machine phase windings," in *Proc. Int. Naval Eng. Conf. (INEC)*, Glasgow, U.K., 2014, pp. 707–718.

[24] J. F. Eastham, T. Cox, and J. Proverbs, "Application of planar modular windings to linear induction motors by harmonic cancellation," *IET Electr. Power Appl.*, vol. 4, no. 3, p. 140, Mar. 2010, doi: 10.1049/iet-epa.2009.0086.


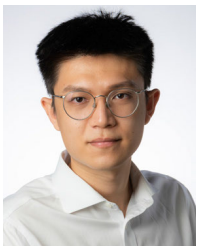

**HAN WANG** received the M.Sc. degree from the University of Bath, Bath, U.K., in 2019, where he is currently pursuing the Ph.D. degree with the Department of Mechanical. His research interests include axial flux permanent magnet design and control and dual wound machine design.

**XIANWU ZENG** (Member, IEEE) received the M.Sc. and Ph.D. degrees from The University of Manchester, in 2009 and 2014, respectively. He had a broad industry experience in power converter design. He was a lead power electronics engineer in GE grid solution before and was responsible to design valve unit for HVDC projects. He was also involved in several automotive projects including kW level dc–dc converter and inverter. In 2019, he joined the University of Bath, as a Lecturer. His research interests include power electronics, motor drives, hybrid electric vehicles, and renewable energy interface systems.

**JOHN FREDERICK EASTHAM** was the Head of Department, the Dean, and the Pro-Vice-Chancellor at the University of Bath, where he is currently an Emeritus Professor. He is also a consultant to several manufacturing companies. He is a fellow of the Royal Academy of Engineering and the Royal Society of Edinburgh.

**BOYUAN YIN** received the joint B.Eng. degree from North China Electric Power University, Beijing, China, and the University of Bath, U.K., in 2018, and the Ph.D. degree from the University of Bath. His research interests include hybrid dc circuit breaker and electric machine design.

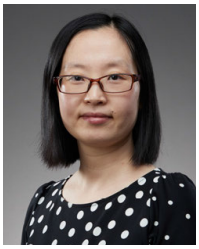

**XIAOZE PEI** (Senior Member, IEEE) received the B.Eng. and M.Eng. degrees from Beijing Jiaotong University, Beijing, China, in 2006 and 2008, respectively, and the Ph.D. degree from The University of Manchester, Manchester, U.K., in 2012. She was a Research Associate at the University of Manchester. In 2017, she joined the University of Bath, as a Lecturer, a Reader (an Associate Professor), in 2022, and a Professor of transport electrification, in 2023. Her research interests include hydrogen-powered electric aircraft and novel electric machine design.